Articles

The Origin of the Metal-insulator Transitions in Non-stoichiometric $TlCu_{3-x}S_2$ and α-$BaCu_{2-x}S_2$

Dongwoon Jung,* Hyun-Guk Choi, and Hanjin Kim

Department of Chemistry and the Institute of Natural Basic Sciences, Wonkwang University, Iksan, Jeonbuk 570-749, Korea
**E-mail: djung@wonkwang.ac.kr*
Received November 7, 2005

The structure-property relations of ternary copper chalcogenides, $TlCu_{3-x}S_2$ and α-$BaCu_{2-x}S_2$ are examined. The density of states, band dispersions, and Fermi surfaces of these compounds are investigated to verify the reason of the metal-insulator transitions by extended Huckel tight-binding band calculations. The origin of the metal-insulator transitions of non-stoichiometric $TlCu_{3-x}S_2$ and α-$BaCu_{2-x}S_2$ is thought to be the electronic instability induced by their Fermi surface nesting.

Key Words : Metal-insulator transition, Fermi surface nesting

Introduction

Ternary copper chalcogenides exhibit a large variety of anomalies in physical properties. Both $K_3Cu_8S_6$[1,2] and ACu_7S_4 (A=K, Tl)[3,4] exhibit resistivity anomalies and superlattice modulations, whereas $Na_3Cu_4S_4$ does not[5] despite its one-dimensional (1D) metallic character.[6] $TlCu_{7-x}S_4$, as a quasi-one dimensional sulfide, exhibits successive phase transitions at 60, 165, 190, 220, 245, and 395 K.[3,4] Electron diffraction study on this compound also shows the evidence of superlattice modulations at 165 and 245 K. Similar results are collected in the isostructural phases $KCu_{7-x}S_4$ and $RbCu_{7-x}S_4$.[3,4] In addition, phase transitions can be found in other copper chalcogenide, α-$BaCu_{4-x}S_3$ at 190 K.[7] The origin of the superlattice modulations in copper chalcogenides is rather diverse. DiSalvo and Sato groups suggest that $K_3Cu_8S_6$ shows charge density wave (CDW)-like phase transitions at 55 K and 153 K,[1,2,8] while Whangbo and his coworkers claim that the phase transitions of $K_3Cu_8S_6$ and ACu_7S_4 (A=K, Tl, Rb) originate not from the CDW instability but from the ordering of copper atoms.[9,10]

Recently Ohtani *et al.* reported the electrical properties and phase transitions of $TlCu_{3-x}S_2$ and $BaCu_{2-x}S_2$.[11] The oxidation states of $TlCu_3S_2$ and $BaCu_2S_2$ can be described as $(Tl^+)(Cu^+)_3(S^{2-})_2$ and $(Ba^{2+})(Cu^-)_2(S^{2-})_2$. The valence bands of these compounds consist of mainly the Cu d-orbital block. In the above oxidation state scheme, all Cu d-orbitals are occupied with d^{10} electronic configuration. Therefore, stochiometric ternary copper sulfides are non-metals by definition that there is no partially filled band. However, similarly to other ternary sulfides $ACu_{7-x}S_4$ (A=K, Tl, Rb), the non-stoichiometric $TlCu_{3-x}S_2$ and α-$BaCu_{2-x}S_2$ become metallic and show phase transitions. This was recently shown by Ohtani *et al.* who prepared both stoichiometric and non-stoichiometric $TlCu_{3-x}S_2$ and α-$BaCu_{2-x}S_2$ using solid state reaction, and found that these two compounds exhibit metal-insulator transitions at 120 K and 200 K, respectively. They suggested that the origin of the phase transition of $TlCu_{3-x}S_2$ would be an electron correlation effect which occasionally causes the Mott transition, while that of α-$BaCu_{2-x}S_2$ is not yet clear. In the present work, we calculate the electronic structure of $TlCu_{3-x}S_2$ and $BaCu_{2-x}S_2$ using the extended Huckel tight-binding (EHTB) method[12] to investigatethe origin of the phase transitions of the compounds. The atomic orbital parameters used in the calculation are given in Table 1.

Table 1. Atomic Orbital Parameters used in EHTB Calculations[a]: Valence orbital Ionization Potential H_{ii}(eV) and Exponent of the Slater-type Orbital ζ

atom	orbital	H_{ii}(eV)	ζ_1 (c_1)	ζ_2 (c_2)
Cu	3d	−14.0	5.95 (0.5933)	2.30 (0.5744)
	4s	−11.4	2.2000)	
	4p	−6.06	2.20 (1.00)	
S	3s	−20.0	2.122(1.00)	
	3p	−13.3	1.827(1.00)	
Tl	6s	−11.6	2.30(1.00)	
	6p	−5.80	1.60(1.00)	

[a]Parameters are collected from the following data: (a) Clementi, E.; Roetti, C. *Atomic Data Nuclear Data Tables* **1974**, *14*, 177. (b) McLeen, A. D.; McLeen, R. S. *Atomic Data Nuclear Data Tables* **1981**, *26*, 197. (c) Richardson, J. W.; Blackman, M. J.; Ranochak, J. E. *J. Chem. Phys.* **1973**, *58*, 3010.

Structures. $TlCu_{3-x}S_2$ consists of Cu_4S_4 columns running along the crystallographic b-axis as shown in Figure 1a.[13] Every copper atom in Cu_4S_4 unit is coordinated by three sulfur atoms, as shown in Figure 1b. Between two Cu_4S_4 units, there are two copper atoms each of which is connected to three sulfur atoms, two in adjacent Cu_4S_4 unit and one in the next Cu_4S_4 unit. Consequently, two CuS_3 units construct

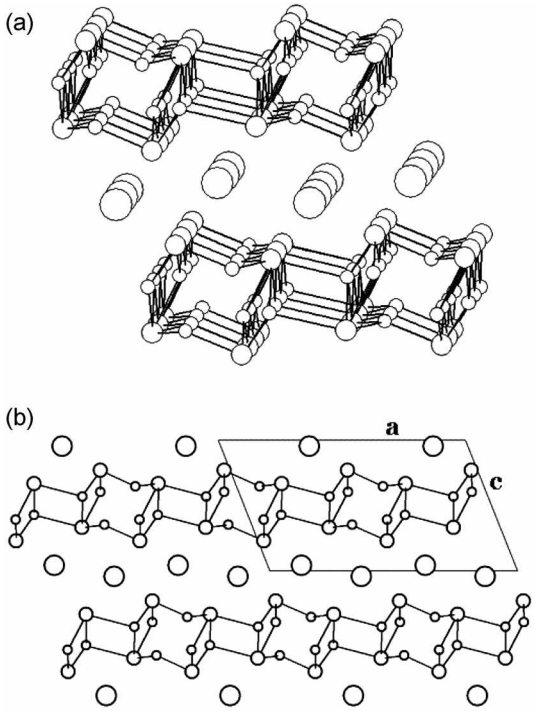

Figure 1. Structures of $TlCu_{3-x}S_2$ (a) projected along the b-axis and (b) three dimensional shape. Small, medium, and large circles represent Cu, S, and Tl atoms, respectively.

the edge-sharing tetrahedra. [hereafter the copper atoms of Cu_4S_4 columns are referred to as Cu(1) atoms and those of the tetrahedral chains are the Cu(2) atoms]. So it is convenient to represent $TlCu_3S_2$ as $Tl_2(Cu_4S_4)(Cu_2)$ in a unit cell. The $(Cu_4S_4)(Cu_2)$ unit is repeating infinately along the a-axis and hence, the compound shows layered structure. Each layer is separated by thallium atoms, as shown in Figure 1. The number of Cu(2) atoms in $TlCu_3S_2$ per unit cell are smaller than those in $K_3Cu_8S_6$ by 1 and the rest of the structure is similar. In a non-stoichiometric $TlCu_{3-x}S_2$, vacancy in Cu(2) atom site increases as increasing the x value. The interatomic distances indicate that the bonding in the compound has partial ionic and partial covalent character. The Tl-S distances, for instance, are near the sum of the ionic radii of S2- and monovalent Tl^+ [*i.e.*, d(Tl-S) = 3.33 Å, $(r_{Tl} - r_S)_{ionic}$ = 3.33 Å] whereas the Cu-S distances are a little beyond the covalent radii sum of Cu and S [*i.e.*, d(Cu-S) = 2.32 Å, $(r_{Cu} + r_S)_{covalent}$ = 2.19 Å].

$BaCu_{2-x}S_2$ exhibits two different phases α- and β-form. In the α-phase, a Cu_4S_4 unit forms a distorted octagon which is similar to the chair shape. Each Cu_4S_4 unit is edge-shared with the next unit along both a- and b-directions.[14-17] Two CuS_3tetrahedra are also edge-shared along the diagonal directions as shown in Figure 2. Cu_4S_4octagon is connected continuously along the c-direction by forming trigonal prisms of anions thereby constructing the infinite tube by sharing their basal faces. Ba atoms sit at the center of the tube, as shown in Figure 2. Two tetrahedral holes which are occupied by Cu atoms are made at the center of adjacent four tubes by sharing two edges in neighboring tubes. The

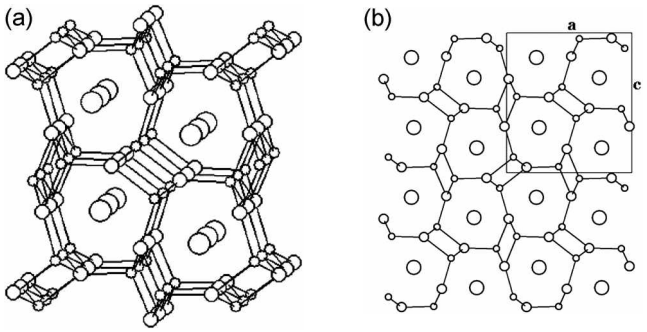

Figure 2. Structure of (a) α-$BaCu_{2-x}S_2$ projected along the b-axis and (b) three dimensional shape. Small, medium, and large circles represent Cu, S, and Ba atoms, respectively.

Cu atoms construct zigzag chains of CuS_4 tetrahedra, which are formed by sharing two adjacent edges of each tetrahedron. All Cu and S in Cu_4S_4 units are occupied in constructing the Cu_4S_4 tube and the CuS_3 tetrahedra. Differently from $TlCu_3S_2$, therefore, there is no differentiation of Cu(1) and Cu(2) in α-$BaCu_{2-x}S_2$. Similarly to $TlCu_{3-x}S_2$, there are ionic and covalent characters in α-$BaCu_{2-x}S_2$. The Tl-S distances ranging from 3.09 Å to 3.29 Å which are shorter than the ionic radii sum of Tl and S indicate that those bonds are ionic, whereas the Cu-S distances ranging from 2.37 Å to 2.55 Å are larger well beyond the covalent radii sum of Cu and S which means that the weak covalent character exists.

Electrical properties. Electrical resistivity ρ as a function of temperature on cooling of $TlCu_{3-x}S_2$ (x = 0, 0.05, 0.07, 0.09) is shown in Figure 3a.[11] As expected from the electronic structure, the stoichiometric $TlCu_3S_2$ (*i.e.*, x = 0) shows insulating behavior within the whole temperature range. However, the samples with Cu(2) vacancy (*i.e.*, x = 0.05, 0.07, and 0.09) exhibit metallic character above 120 K, which means that resistivity of these samples increases with temperature. In the long run, $TlCu_{3-x}S_2$ (x = 0.05, 0.07, and 0.09) samples show a metal-insulator transition at 120 K. Although the metal-insulator transition is not shown, the resistivity of the stoichiometric sample also increases abruptly below this temperature. Interestingly, the resistivity is reduced as x increases up to 0.07, and futher Cu(2) removal results in the increase of the resistivity again. The resistivity data for α-$BaCu_{2-x}S_2$ are shown in Figure 3b.[11] In this compound, the samples having Cu(2) vacancy show a metal-insulator transition at 200 K. Differently from $TlCu_{3-x}S_2$, the resistivity of α-$BaCu_{2-x}S_2$ is continuously getting smaller as x (*i.e.*, hole density) increases.

Electronic structure. The DOS and the projected density of states (PDOS) for the Cu and S atoms in $TlCu_{3-x}S_2$ and α-$BaCu_{2-x}S_2$ are shown in Figures 4a and 4b, respectively. The vertical dashed lines represent the Fermi energies of stoichiometric $TlCu_3S_2$ and α-$BaCu_2S_2$. At the Fermi energy, the DOS values for the stoichiometric samples are both zero, which means that stoichiometric $TlCu_3S_2$ and α-$BaCu_2S_2$ are non-metallic as expected. The resistivity of $TlCu_{3-x}S_2$ and α-$BaCu_{2-x}S_2$ at room temperature are about 0.016 W.cm and 3.98 W.cm, respectively. These values are

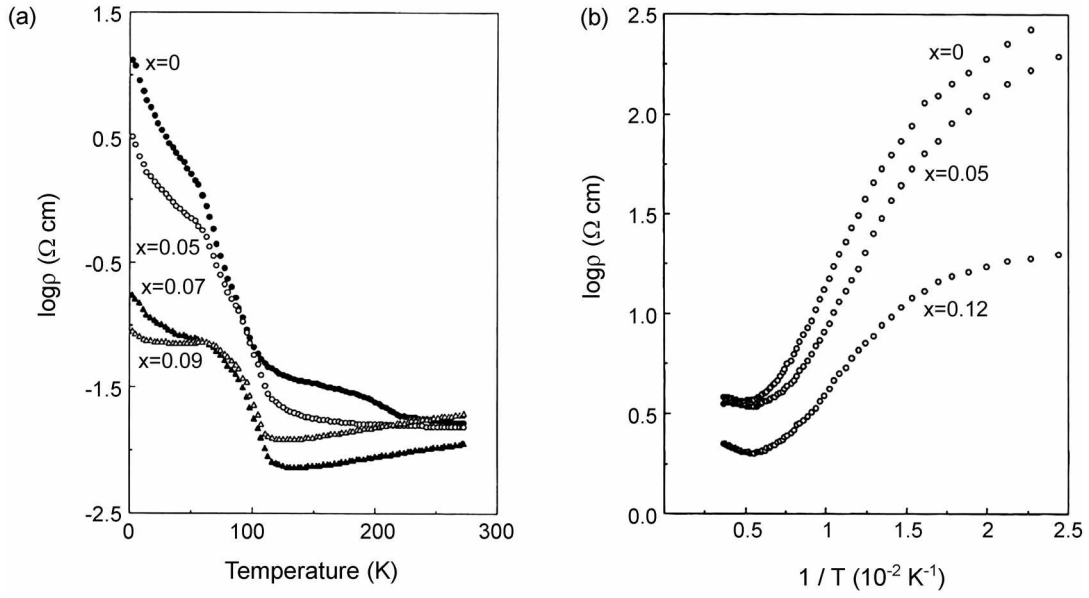

Figure 3. Electrical resistivity of (a) $TlCu_{3-x}S_2$ and of (b) α-$BaCu_{2-x}S_2$ according to the variation of x. These data are taken from the reference [11].

consistent with the band gaps depicted in the DOS figures. Cu vacancies in both samples create the partially filled bands, thereby changing those compounds be metallic. Cu vacancy is nothing more than the electron deficiency in a unit cell. Since the orbitals of the Cu atoms do not contribute much to the top portion of the bands as shown in the PDOS figures, the electronic structures of non-stoichiometric $TlCu_{3-x}S_2$ and α-$BaCu_{2-x}S_2$ can be analyzed by simply lowering the Fermi energy according to the x values (*i.e.*, 0.05 × 11 and 0.07 × 11 electrons per formula unit for x = 0.05 and 0.07 in $TlCu_{3-x}S_2$, respectively. Same electron counting is applied for α-$BaCu_{2-x}S_2$).

Electrical resistivity of non-stoichiometric $TlCu_{3-x}S_2$ (x = 0.05, 0.07, 0.09) is reduced up to x = 0.07 but it goes up again according to further removal of Cu (*i.e.*, x > 0.07), while that of α-$BaCu_{2-x}S_2$ is reduced continuously as x increases. In other words, electrical conductivity of $TlCu_{3-x}S_2$ increases up to x = 0.07 then decreases afterwards, while that of α-$BaCu_{2-x}S_2$ increases continuously within the experimental range of x. Generally electrical conductivity is strongly related to the DOS value around the Fermi energy. As shown in Figure 4a, the DOS of $TlCu_{3-x}S_2$ increases with increasing x values until the Fermi energy goes down to –9.5 eV and then it decreases as the Fermi energy goes down further. Although not shown, the Fermi energy of $TlCu_{3-x}S_2$ at x = 0.7 is about –9.5 eV. The DOS profile of $TlCu_{3-x}S_2$ well explains why the conductivity maximum exists in the compound. On the contrary, DOS of α-$BaCu_{2-x}S_2$ compounds increases steadily as x increases (see Fig. 4b). This result is consistent with the experimental resistivity

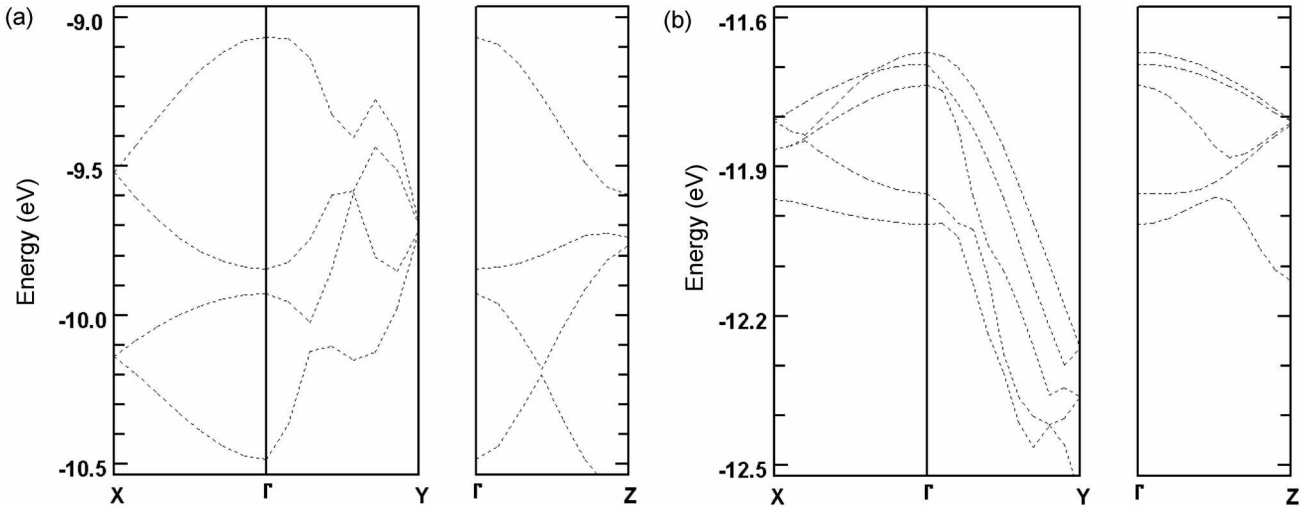

Figure 4. Band dispersions calculated for (a) $TlCu_{3-x}S_2$ and (b) α-$BaCu_{2-x}S_2$ where Γ, X, Y and Z represent the wave vector points (0, 0, 0), (a^*/2, 0, 0), (0, b^*/2, 0), (0, 0, c^*/2) in the first Brillouin zone of the reciprocal lattice, respectively.

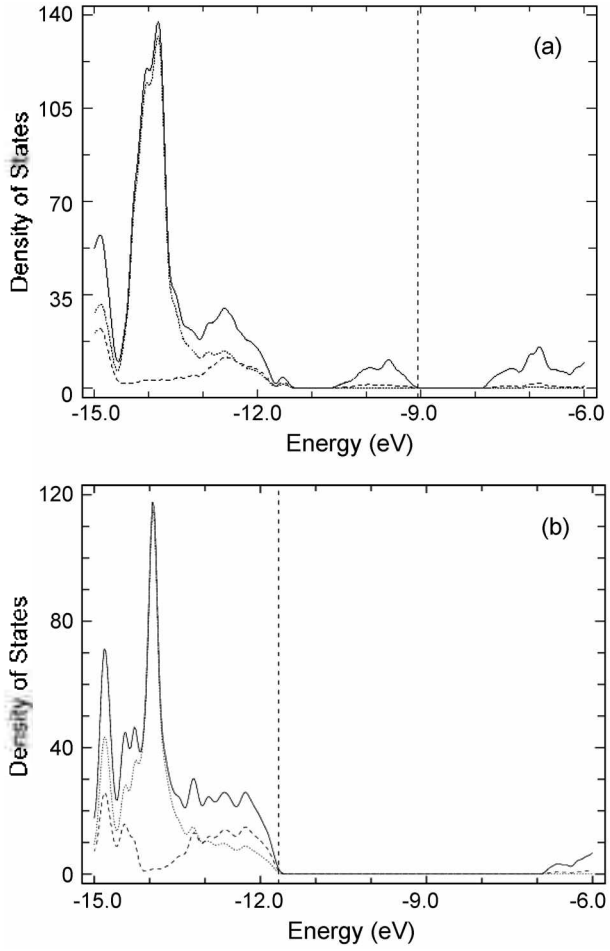

Figure 5. Projected density of states (PDOS) calculated for (a) $TlCu_{3-x}S_2$ and (b) α-$BaCu_{2-x}S_2$. The dotted line, dashed line represent the contributions of Cu 3d and S orbitals, and the solid line represents the total DOS.

measurement data.

Band dispersions calculated for $TlCu_{3-x}S_2$ and α-$BaCu_{2-x}S_2$ are shown in Figures 5a and 5b, respectively. Γ, X, Y, Z represent the wave vector points (0, 0, 0), (a^*/2, 0, 0), (0, b^*/2, 0), (0, 0, c^*/2) in the first Brillouin zone of the reciprocal lattice, respectively. Bands are similarly dispersive along the a-, b-, and c-directions in $TlCu_{3-x}S_2$ while they are strongly dispersive only along the b-direction in α-$BaCu_{2-x}S_2$. Structural features suggest that $TlCu_{3-x}S_2$ may be 2-dimensional since it is a layered compound. Band dispersion of this compound, however, tells us that this compound is 3-dimensional by forming strong interactions between thallium and sulfur atoms in layers of both sides as pointed out in the structure analysis (See Figure 1). α-$BaCu_{2-x}S_2$ seems to be 3-dimensional from the view point of structural aspects (See Figure 2). However, its band dispersion curve suggests that the orbital interactions along the chain direction (*i.e.*, crystallographic b-direction) are stronger than the other two directions. The Fermi surface of a partially filled band is defined as the boundary surface of wave vectors that separate the wave vector region of filled band levels from that the wave vector region of unfilled band

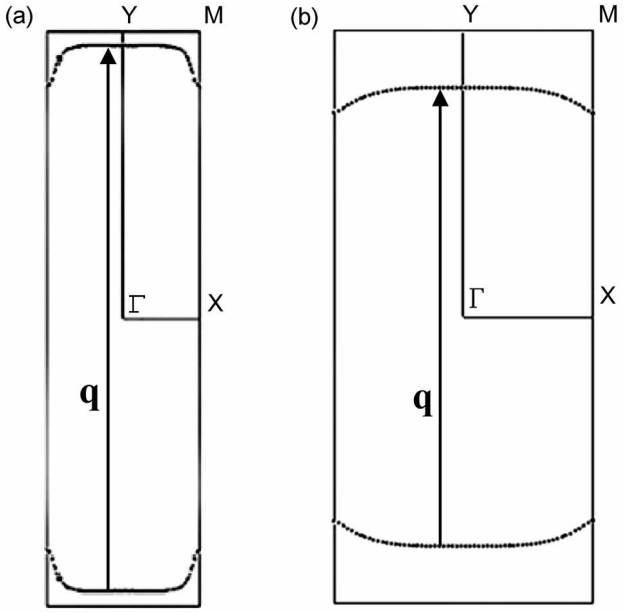

Figure 6. (a) Fermi surface of $TlCu_{3-x}S_2$ associated with the band dispersion cut by the Fermi energy when x = 0.07, (b) Fermi surface of α-$BaCu_{2-x}S_2$ associated with the band dispersion cut by the Fermi energy when x = 0.12.

levels. Since there are several bands cut by the Fermi energy, many Fermi surfaces can be drawn according to the x values for both $TlCu_{3-x}S_2$ and α-$BaCu_{2-x}S_2$. Among them, the representative Fermi surfaces calculated for $TlCu_{3-x}S_2$ and α-$BaCu_{2-x}S_2$ are shown in Figures 6a and 6b when x = 0.07 and x = 0.12,respectively. One piece of a Fermi surface may be superimposable, by translating it with wave vector **q**, onto another piece of the Fermi surface. In such a case, the two pieces are said to be nested by the wave vector **q**. A metallic system with a nesting vector **q** gives rise to a CDW of wave vector **q**, which can be detected by diffuse X-ray scattering as diffuse reflections in between the main Bragg reflections.[18] Essentially two Fermi surfaces given in the Figures 6a and 6b are one-dimensional in nature. Generally, a compound that possesses one-dimensional property shows well nested Fermi surfaces and finally exhibits higher susceptibility to a metal-insulator transition. In both compounds, the Fermi surface nesting phenomena exist with the nesting vectors $\mathbf{q}=0.943\mathbf{b}^*$ in $TlCu_{3-x}S_2$ and $\mathbf{q}=0.80\mathbf{b}^*$ in α-$BaCu_{2-x}S_2$, as illustrated by arrow in Figure 6. Although not shown, the Fermi surface nesting phenomena occur at different x values and different bands with different **q**. The electronic instability induced by these Fermi surface nestings may cause the charge density waves (CDWs) and hence the non-stoichiometric $TlCu_{3-x}S_2$ and α-$BaCu_{2-x}S_2$ exhibit the metal-insulator transitions at 120 K and 200 K, respectively. To verify the origin of the phase transition in $TlCu_{3-x}S_2$ and α-$BaCu_{2-x}S_2$ more clearly, the crystal data below the transition temperature are needed.

Conclusions

The origin of the metal-insulator transitions exhibited in

the ternary copper chalcogenides are still going into controversy. According to the EHTB calculations of the non-stoichiometric $TlCu_{3-x}S_2$ and α-$BaCu_{2-x}S_2$, the Fermi surfaces of both compounds possess one-dimensional property and are partially nested. In the long run, the electronic instability caused by the Fermi surface nesting may be the origin of the metal-insulator transitions of these compounds. The electrical resistivity data obtained from the experimental procedure are well explained with calculated DOS results. The DOS value increases with increasing x up to $x = 0.07$, then decreases beyond $x = 0.07$ in $TlCu_{3-x}S_2$. The electrical resistivity of this compound show same pattern. In α-$BaCu_{2-x}S_2$, however, the DOS value increases continuously according to x value, which is consistent with resistivity experiments.

Acknowledgement. This work is supported by Wonkwang University Research Grant at the year of 2004.

References

1. ter Haar, L. W.; DiSalvo, F. J.; Bair, H. E.; Fleming, R. M.; Waszczak, J. V.; Hatfield, W. E. *Phys. Rev.* **1987**, *B35*, 1932.
2. Fleming, R. M.; ter Haar, L. W.; DiSalvo, F. J. *Phys. Rev.* **1987**, *B35*, 5388.
3. Ohtani, T.; Ogura, J.; Sakai, M.; Sano, Y. *Solid State Commun.* **1991**, *78*, 913.
4. Ohtani, T.; Ogura, J.; Yoshihara, H.; Yokada, Y. *J. Solid State Chem.* **1995**, *115*, 379.
5. Peplinski, Z.; Brown, D. B.; Watt, T.; Hatfield, W. E.; Day, P. *Inorg. Chem.* **1982**, *21*, 1752.
6. Whangbo, M.-H.; Canadell, E. *Inorg. Chem.* **1990**, *29*, 1395.
7. Ohtani, T.; Hoshino, T.; Tsujinouchi, A.; Hasegawa, M.; Nagaoka, N.; Yokota, Y.; Okada, Y. *Mater. Res. Bull.* **1995**, *30*, 161.
8. Sato, H.; Igaki, E.; Nakamura, T.; Ban, T.; Kojima, N. *Solid State Commun.* **1989**, *71*, 793.
9. Whangbo, M.-H.; Canadell, E. *Sold State Commun.* **1992**, *81*, 895.
10. Lee, K.-S.; Seo, D.-K.; Whangbo, M.-H.; Li, H.; Mackay, R.; Hwu, S.-J. *J. Solid State Chem.* **1997**, *134*, 5.
11. Ohtani, T.; Takeuchi, H.; Koh, K.; Kaneko, T. *J. Alloys and Compounds* **2001**, *317-318*, 201-207.
12. Whangbo, M.-H.; Hoffmann, R. *J. Am. Chem. Soc.* **1978**, *100*, 6093.
13. Klepp, K.; Yvon, K. *Acta Cryst.* **1980**, *B36*, 2389.
14. Iglesias, J. E.; Pachali, K. E.; Steinfink, H. *J. Solid State Chem.* **1974**, *9*, 6.
15. Iglesias, J. E.; Steinfink, H. *Z. Kryst. Bd.* **1975**, *142*, S.308.
16. Saeki, M.; Onoda, M.; Nozaki, H. *Mat. Res. Bull.* **1988**, *23*, 603.
17. Onoda, M.; Saeki, M. *Mat. Res. Bull.* **1989**, *24*, 1337.
18. Moret, R.; Pouget, J. P. In *Crystal Chemistry and Properties of Materials with Quasi-One-Dimensional Structures*; Rouxel, J., Ed.; Reidel: Dordrecht, The Netherlands, 1986; p 87.